Surface Science xxx (2016) xxx–xxx

Contents lists available at ScienceDirect

Surface Science

journal homepage: www.elsevier.com/locate/susc

Formaldehyde adsorption and decomposition on rutile (110): A first-principles study

Liming Liu [a], Jin Zhao [a,b,c,d,*]

[a] Hefei National Laboratory for Physical Sciences at Microscale and Department of Physics, University of Science and Technology of China, Hefei, Anhui 230026, P.R. China
[b] Synergetic Innovation Center of Quantum Information & Quantum Physics, University of Science and Technology of China, Hefei, Anhui 230026, China
[c] Key Laboratory of Strongly-Coupled Quantum Matter Physics, Chinese Academy of Sciences, School of Physical Sciences, University of Science and Technology of China, Hefei, China
[d] Department of Physics and Astronomy, University of Pittsburgh, Pittsburgh, PA, USA

ARTICLE INFO

Available online xxxx

Keyword:
DFT
Formaldehyde decomposition
Photocatalytic reactivity

ABSTRACT

We investigated the adsorption and decomposition of formaldehyde (HCHO) molecule on stoichiometric rutile TiO_2(110) surface using first principles-calculations. By comparing the adsorption energy of one bidentate and two monodentate configurations, we found the bidentate configuration is the most stable one because of an additional C-O bond formation. The monodentate configuration can change into the bidentate configuration by overcoming a small barrier less than 0.1 eV. Then, we investigated the decomposition of HCHO which involves two deprotonation processes starting from different adsorption structures. The energy barrier of the first deprotonation is 1.3 eV and 1.1 eV for bidentate and monodentate configurations. After the first deprotonation, an adsorbed formate HCOO specie is formed. The second deprotonation needs 1.74 eV and 1.64 eV for bidentate and monodentate configurations, respectively. After that, an adsorbed CO_2 is formed. It can desorb from the surface after overcoming a small barrier of 0.12 eV. In principle, it is also possible to obtain a CO molecule from the surface. Yet a large energy barrier higher than 1.74 eV needs to be overcome. By analyzing the energy level alignment of molecular orbitals with TiO_2 energy band edges, we discussed the photocatalytic activity of the reactants and intermediates during the decomposition process. Our results give a clear description of the adsorption structure and thermal decomposition process of HCHO on rutile TiO_2(110) surface. The discussion of photocatalytic reactivity based on energy level alignment provides valuable insights to understand the combined photocatalytic and thermally catalytic reactions.

1. Introduction

TiO_2 surfaces have important applications in photovoltaics, heterogeneous catalysis and photocatalysis due to their chemical stability, high photoelectric conversion efficiency, non-toxicity and low cost [1–6]. A good understanding of intrinsic physical and chemical processes on pristine TiO_2 surfaces is thus essential for the development of these applications [7–13]. J.T. Yates, among others, has contributed significantly to the fundamental surface science studies on TiO_2 [14–18].

Formaldehyde (HCHO), as the simplest aldehyde, is a common toxic pollutant that can lead to severe health issues; besides, it is an important precursor for organic synthesis. Heterogeneous photocatalytic oxidation using TiO_2 is becoming an attractive technique for the degradation of airborne contaminants such as formaldehyde [19]. Formaldehyde is known as the product of methanol oxidation on TiO_2 surface [20–22]. Recent thermal desorption spectroscopy (TPD) and X-ray photoelectron spectroscopy (XPS) investigations by W. Huang et al. and X. Yang et al. showed that during photocatalytic and thermal catalytic surface reactions, HCHO produces C_2H_4, CO, CO_2 and CH_3OH on rutile TiO_2(110) at different temperatures. The adsorbed formate (HCOO) and HCO are important intermediates in the reaction [21,23,24]. C.M. Friend et al. discovered that transient HCO is generated photochemically from formaldehyde and then it couples with residual methoxy on the surface to yield methyl formate [25]. Z. Zhang et al. studied the adsorption and diffusion of HCHO on TiO_2 surface using atomic resolved scanning tunneling microscopy (STM) [26–28]. There are also several theoretical works on HCHO adsorption on TiO_2 [29–31]. For example, Kieu et al. proposed an adsorption model of HCHO on TiO_2(110) and (001) surfaces based on density functional theory (DFT) calculations. Chemical monodentate adsorption structures by forming O-Ti bond with oxygen of HCHO and five-fold-coordinated titanium (Ti_{5c}) of substrate have adsorption energies about −0.68 eV [29]. Haubrich et al. proposed a new bidentate adsorption configuration with oxygen of HCHO bonded to Ti_{5c} and carbon of HCHO bonded to a neighboring bridge bonded oxygen (O_b) [30]. The adsorption energy of bidentate configuration is about 0.6 eV lower than monodentate configurations proposed by Kieu et al. A new bidentate adsorption configuration with oxygen of HCHO bonded to Ti_{5c} and carbon of HCHO bonded to surface-in-plane oxygen of TiO_2 substrate proposed by Liu et al. has

* Corresponding author.
E-mail address: zhaojin@ustc.edu.cn (J. Zhao).

http://dx.doi.org/10.1016/j.susc.2015.12.036
0039-6028/

the adsorption energy close to monodentate adsorption configuration [31]. Zhang et al. and Haubrich et al. studied the effects of oxygen vacancy on the adsorption [28,30,32]. The diffusion barrier of HCHO on TiO_2 is also studied with DFT [32].

Most of the existing theoretical works focus on the adsorption structure of HCHO on rutile TiO_2(110) surface [29–31]. However, the thermal catalytic and photocatalytic reaction mechanism of HCHO on this surface is still unclear. In this work, we first confirmed the adsorption structures of HCHO on stoichiometric rutile TiO_2(110) surface. One bidentate and two monodentate configurations are studied. Then, we investigated the thermal reaction pathways of HCHO decomposition to CO_2 and CO starting from different initial adsorption structures. Our study shows that the energy barrier of the deprotonation of the first H is 1.3 eV and 1.1 eV for bidentate and monodentate configurations. After that, an adsorbed formate $HCOO_b$ specie is formed. The deprotonation of the second H needs 1.74 eV and 1.64 eV for bidentate and monodentate configurations. CO_2 can be separated from the surface by overcoming a small barrier of 0.12 eV afterwards. In contrast, to separate CO from the surface, an energy barrier around 1.8 eV needs to be overcome. By analyzing the energy level alignment of molecular orbitals with TiO_2 energy band edges, we discussed the photocatalytic activity of the reactants and intermediates during the decomposition process. Our results give a clear description of the adsorption structures and thermal decomposition process of HCHO on rutile TiO_2(110) surface. The photocatalytic reactivity discussion based on energy level alignment provides valuable insights to understand the combined photocatalytic and thermal catalytic reactions.

2. Calculation details

We performed periodic DFT calculations by using the Vienna Ab-initio Simulation Package (VASP) [33,34]. The generalized gradient approximation (GGA) functional was adopted with the Perdew–Burke–Ernzerhof (PBE) exchange-correlation description [35,36]. The energy cutoff of 400 eV for plane-wave basis sets was used to expand the electronic wave function with valence configuration of C-$2s^2 2p^2$, H-$1s^1$, O-$2s^2 2p^4$ and Ti-$4s^2 3d^2$. The projector augmented wave (PAW) method was used to describe the electron–ion interaction [37,38]. Dipole moment corrections were adopted to cancel the interactions between the slab and its periodic images for all calculations. The structure was optimized until the force on each atom was smaller than 0.02 eV/Å. A slab containing 3 Ti-O-Ti tri-layers was applied. The atoms in the bottom Ti-O-Ti tri-layer were fixed to the positions within bulk TiO_2 during the structure optimization. To avoid the interlayer interaction, we added a vacuum of 15 Å between the slabs. A surface supercell of (5×2) was used to investigate the HCHO reaction pathway. Nudged elastic band (NEB) [39] method was adopted to search reaction paths of HCHO decomposing to CO or CO_2. During the optimization and NEB calculations, only Gamma point was used. For the electronic structure and total energy calculations, $8 \times 4 \times 1$, $4 \times 3 \times 1$ and $3 \times 3 \times 1$ k-point mesh sets were used for 2×2, 3×2 and 5×2 supercells, respectively. To compare the stability of various adsorption structures, we defined the adsorption energy as

$$E_{ads} = E_{HCHO+TiO_2} - E_{HCHO} - E_{TiO_2} \quad (1)$$

3. Results and discussion

3.1. Adsorption configurations

We first studied the adsorption structure of HCHO on TiO_2. HCHO is a planar molecule with C_{2v} symmetry and partially polarized. Oxygen atom of HCHO molecule (O_m) could bind to Ti_{5c} from substrate by forming bond via the hybridization of O_{2p} and Ti_{3d} orbitals. Hydrogen bonds could further stabilize the structure since both O_b and three-fold-coordinated oxygen in plane (O_p) could have dispersive interaction with molecular hydrogen atoms. Besides the Ti_{5c}-O_m bond, the three-fold-coordinated molecular carbon (C_m) could also bind to O_b accompanied by the hybridization of C_m changing from sp^2 to sp^3.

Based on these bond formation analyses, we proposed three adsorption configurations of HCHO on pristine rutile TiO_2(110) as shown in Fig. 1. First, HCHO molecule could adsorb on TiO_2 substrate maintaining its planar configuration by forming Ti_{5c}-O_m bond and a hydrogen bond with O_b or O_p, forming, namely, monodentate configurations. The two kinds of monodentate configurations can be labeled as η^1-O_b and η^1-O_p, respectively (Fig. 1(a,d and b,e)). The two monodentate configurations are almost degenerate in energy as shown in Table 1. The Ti_{5c}-O_m bond length is around 2.2 Å. Then, the bidentate

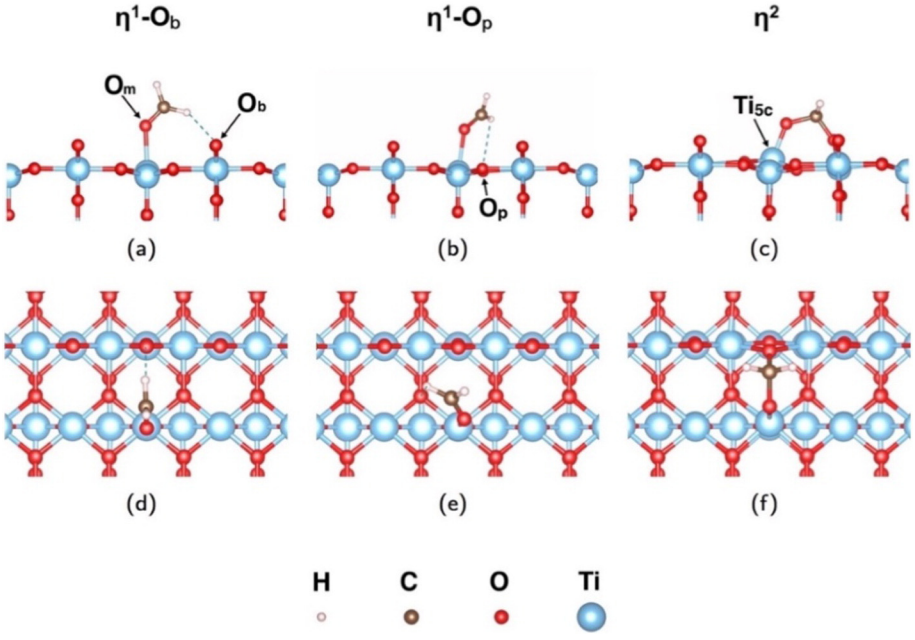

Fig. 1. Adsorption configurations of HCHO on stoichiometric TiO_2(110) surface: (a–c) and (d–f) show the side and top views of monodentate adsorption structure η^1-O_b, η^1-O_p and bidentate adsorption structure η^2.

Please cite this article as: L. Liu, J. Zhao, Formaldehyde adsorption and decomposition on rutile (110): A first-principles study, Surf. Sci. (2016), http://dx.doi.org/10.1016/j.susc.2015.12.036

Table 1
Adsorption energies and Ti_{5C}-O_m bond lengths of HCHO adsorption on stoichiometric TiO_2(110) surface.

Adsorption configurations	E_{ads} (eV) (2 × 2)	E_{ads} (eV) (3 × 2)	E_{ads} (eV) (5 × 2)	Ti_{5C}-O_m (Å) (2 × 2)	Ti_{5C}-O_m (Å) (3 × 2)	Ti_{5C}-O_m (Å) (5 × 2)
η^1-O_b	−0.58	−0.73	−0.73	2.244	2.205	2.198
η^1-O_p	−0.61	−0.76	−0.77	2.237	2.192	2.190
η^2	−1.25	−1.76	−1.81	1.824	1.820	1.818

configuration can be formed by forming two chemical bonds: Ti_{5c}-O_m bond and C_m-O_b bond. It is labeled as η^2 as shown in Fig. 1(c and f). This configuration has a shorter Ti_{5c}-O_m bond (1.82 Å) and an additional C_m-O_b bond (1.42 Å), resulting in the decrease of E_{ads} compared to two monodentate adsorption configurations (Table 1). By forming this bidentate structure, the molecular carbon becomes tetrahedrally coordinated accompanied by the transition of carbon orbital hybridization from sp^2 to sp^3. Our calculation results agree with C.M. Friend's study [30].

In the XPS, TPD and STM measurements, both the monodentate and bidentate configurations have been observed [23,27]. And the monodentate configuration has been observed to be the dominate adsorption [23]. However, in our calculations, the energy difference between the monodentate and bidentate configuration is as large as 1.1 eV for the (5 × 2) supercell (Table 1). Trying to understand this, we checked the influence of HCHO coverage on its adsorption stability. Besides the (5 × 2) super cell (0.1 ML), two more different super cells of 3 × 2 (0.17 ML) and 2 × 2 (0.25 ML) were adopted. Here, 1 ML refers to one HCHO adsorbed on each Ti_{5C} atom. The E_{ads} with different coverage is presented in Table 1. The structures of the three configurations do not change much. And the order of relevant stability also keeps. Yet we found that the bidentate η^2 is more sensitive to the adsorption coverage. The E_{ads} increases a little bit from −1.81 eV to −1.76 eV when the coverage increases from 0.1 ML to 0.17 ML. Then, it increases distinctly to −1.25 eV when the coverage reaches 0.25 ML. In contrast, the two monodentate configurations are less sensitive to the coverage. The increasing of E_{ads} along with the coverage is less than 0.2 eV. With a coverage of 0.25 ML, the energy difference of bidentate η^2 with monodentate η^1-O_b and η^1-O_p is only about 0.6 eV. This can be easily understood from the steric effects aroused by two reasons: (i) the bidentate η^2 configuration has the tetrahedral configuration instead of planar configuration or (ii) the stronger Ti_{5c}-O_m bond in η^2 configuration pulls the Ti_{5c} out of the surface. The large distortion of TiO_2 surface also induces steric effects.

It is possible for the bidentate and monodentate configurations to convert to each other. We calculated the structure conversion energy barriers using (5 × 2) (0.1 ML) and (2 × 2) (0.25 ML) as shown in Fig. 2. One can see that for both cases, the energy barrier between η^1-O_b and η^1-O_p is very small, and is less than 50 meV. Yet the energy barrier between η^1-O_p and η^2 is more sensitive to the coverage. For 0.1 ML, it is as small as 30 meV. For 0.25 ML, the barrier reaches 0.1 eV. The large energy difference and small conversion barrier between bidentate and monodentate configurations could not explain the dominate adsorption of monodentate configuration [23]. Z. Zhang and Q. Ge et al. also discussed the present DFT results are at odds with the experimental observation [26]. We believe that a deeper theoretical investigation, including the effects of oxygen vacancy and Ti interstitial, is further needed.

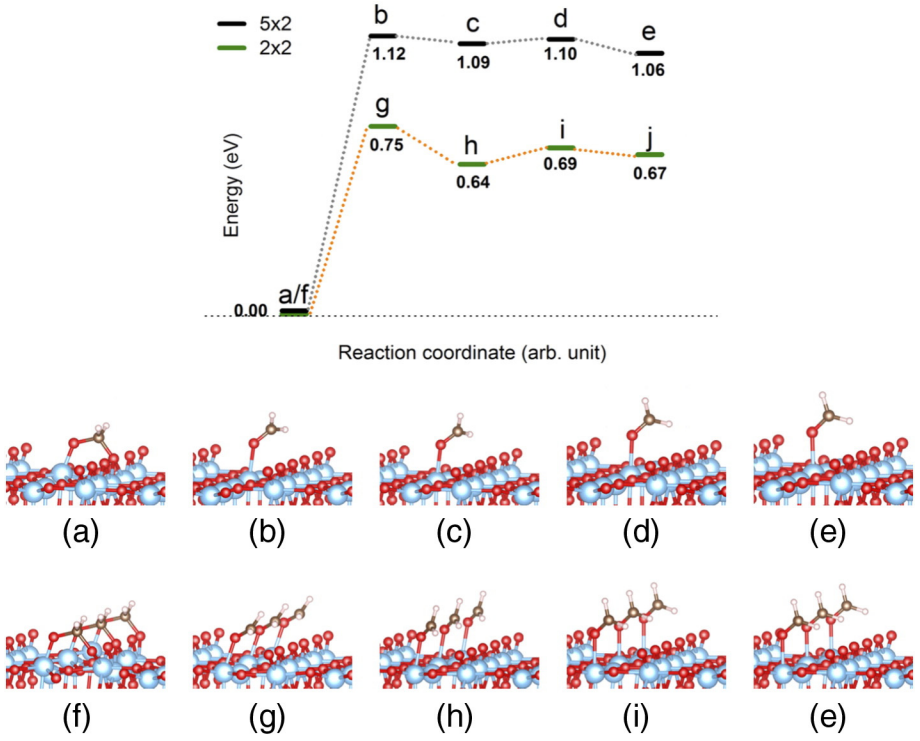

Fig. 2. The reaction pathways and corresponding structures of adsorption configuration conversion from bidentate η^2 to monodentate η^1-O_p then monodentate η^1-O_b of HCHO on stoichiometric TiO_2(110) surface. The results of (5 × 2) and (2 × 2) super cells are shown using the black and green bars.

Please cite this article as: L. Liu, J. Zhao, Formaldehyde adsorption and decomposition on rutile (110): A first-principles study, Surf. Sci. (2016), http://dx.doi.org/10.1016/j.susc.2015.12.036

3.2. Thermal decomposition reaction pathway

After we confirmed the adsorption structures, we studied the decomposition energy barrier of HCHO on rutile TiO_2(110) surface from different adsorption structures. We used (5×2) super cell to investigate the decomposition reaction pathway. The decomposition of HCHO to CO or CO_2 essentially is a two-step deprotonation process. The protons transfer from HCHO to TiO_2 surface to form surface hydroxyls (OH_b) with O_b. First, we studied the decomposition reaction pathway of the most stable η^2 structure. Fig. 3 shows the reaction pathways and corresponding structures. Fig. 3(a–c) show the process of the first deprotonation. The proton transfer from HCHO to a neighboring O_b forming an OH_b. After that, an intermediate formate $HCOO_b$ is formed. During this process, the sp^3 hybridization in η^2 changes to the sp^2 hybridization in adsorbed $HCOO_b$. The energy barrier for the first deprotonation step is 1.3 eV and the adsorbed $HCOO_b$ is 1.4 eV more stable than HCHO adsorbed on TiO_2(110) surface, namely, the first deprotonation is an exothermic reaction. The reverse reaction from $HCOO_b$ to HCHO needs to overcome a large energy barrier of 2.7 eV.

The second deprotonation process first involves breaking of Ti-O_m bond (Fig. 3(d)). After that, by forming two H bonds with the neighboring OH_b and O_b, another intermediate formate $HCOO_b'$ is formed, which is 0.22 eV less stable than the intermediate $HCOO_b$ (Fig. 3(e)). The energy barrier of this process is 0.49 eV. Then, the $HCOO_b'$ is deprotonated by transferring a proton to the other neighboring O_b and forming another OH_b (Fig. 3(e–g)). During this deprotonation process, the O_b where HCO is adsorbed is pulled out of the surface with the Ti-O_b bond increasing from 2.17 Å in Fig. 3(e) to 2.81 Å forming an adsorbed CO_2 in oxygen vacancy on TiO_2 (Fig. 3(g)). The reactant (HCO) and product (CO_2) of this step have almost degenerate energy and the energy barrier is around 1.74 eV. By overcoming a small energy barrier of 20 meV, the CO_2 molecule can desorb easily from the surface (Fig. 3(g, j and k)). In principle, it is also possible to reduce CO_2 to a CO molecule. However, our calculations show that a large barrier of 1.95 eV needs to be overcome to separate CO from the surface (Fig. 3(g–i)). The decomposition of HCHO to CO_2 is an exothermic reaction. The energy difference between the product and the reactant is 1.14 eV.

Then, we study the decomposition HCHO starting from monodentate structures. Since η^1-O_p and η^1-O_b are almost degenerate in energy and the energy barrier between them is very small, we only study the decomposition reaction pathway starting from η^1-O_b as shown in Fig. 4. The first deprotonation process is a proton transfer to a neighboring O_b through the hydrogen bond and forming an OH_b (Fig. 4(a–c)). After that, an intermediate $HCOO_b$ is formed with O_b in an adjacent row which is 2.4 eV lower in energy (Fig. 4(c)). The energy barrier of this process is 1.11 eV. The second deprotonation is a little bit different with the decomposition from η^2 structure. Here, we did not find the formation of stable intermediate $HCOO_b'$. This is because the absent of a neighboring OH_b thus the hydrogen bond between intermediate $HCOO_b'$ and OH_b could not be formed. The intermediate $HCOO_b$ is directly deprotonated into an adsorbed CO_2 (Fig. 4(e)) by overcoming an energy barrier of 1.64 eV. Similarly, the energy barrier to reduce CO_2 to CO is as large as 1.74 eV. (Fig. 4(e–g)) Since η^1-O_b is less stable than η^2, obviously the decomposition from η^1-O_b to CO_2 is also an exothermic reaction. The energy

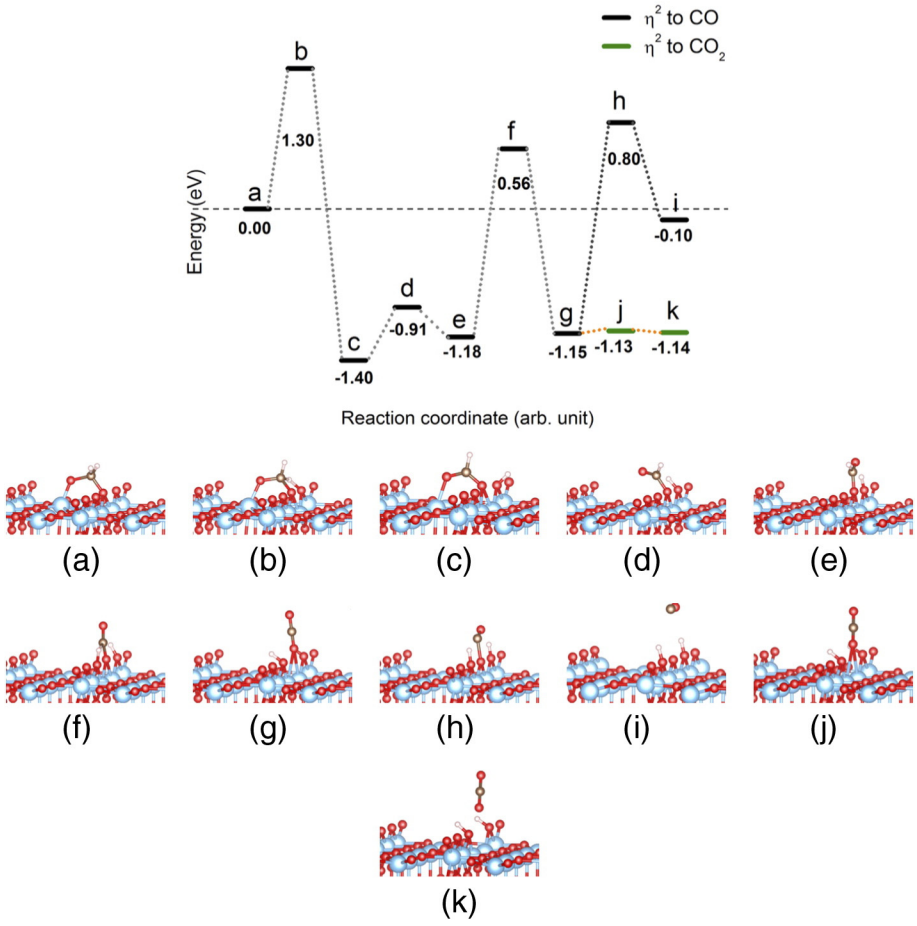

Fig. 3. The reaction pathway and corresponding structures of bidentate η^2 HCHO decomposition to CO_2 and CO structure (c), (e) and (g) correspond to intermediates of $HCOO_b$, $HCOO_b'$ and the adsorbed CO_2.

Please cite this article as: L. Liu, J. Zhao, Formaldehyde adsorption and decomposition on rutile (110): A first-principles study, Surf. Sci. (2016), http://dx.doi.org/10.1016/j.susc.2015.12.036

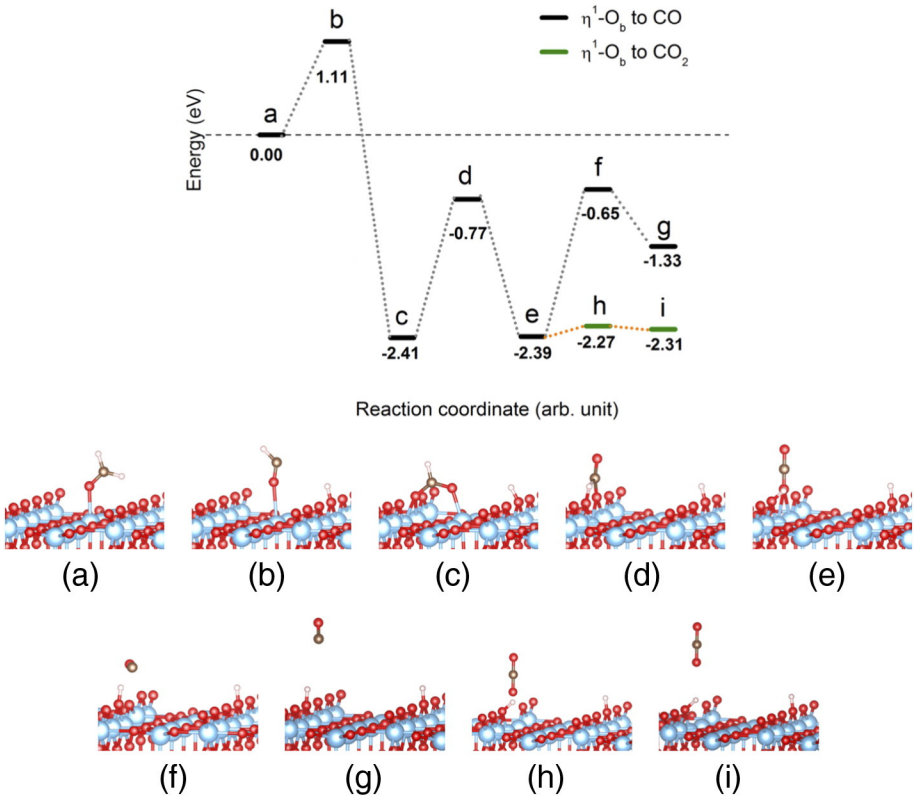

Fig. 4. The reaction pathway and corresponding structure of monodentate η^1-O_b HCHO decomposition to CO_2 and CO. (c) and (e) Corresponds to the intermediate $HCOO_b$ and the adsorbed CO_2.

difference between the product and the reactant is 2.31 eV. The reverse reaction process contains an energy barrier of 3.51 eV from $HCOO_b$ to HCHO.

Our results show that the adsorbed formate $HCOO_b$ and $HCOO_b'$ are two stable intermediates during the decomposition. These results are in agreement with some of the experimental observation [23–25]. Our results also prove that the decomposition of toxic HCHO to non-toxic CO_2 is an exothermic reaction, suggesting that stoichiometric rutile TiO_2(110) surface could be used to decompose HCHO. In contrast, the decomposition to CO is much more difficult.

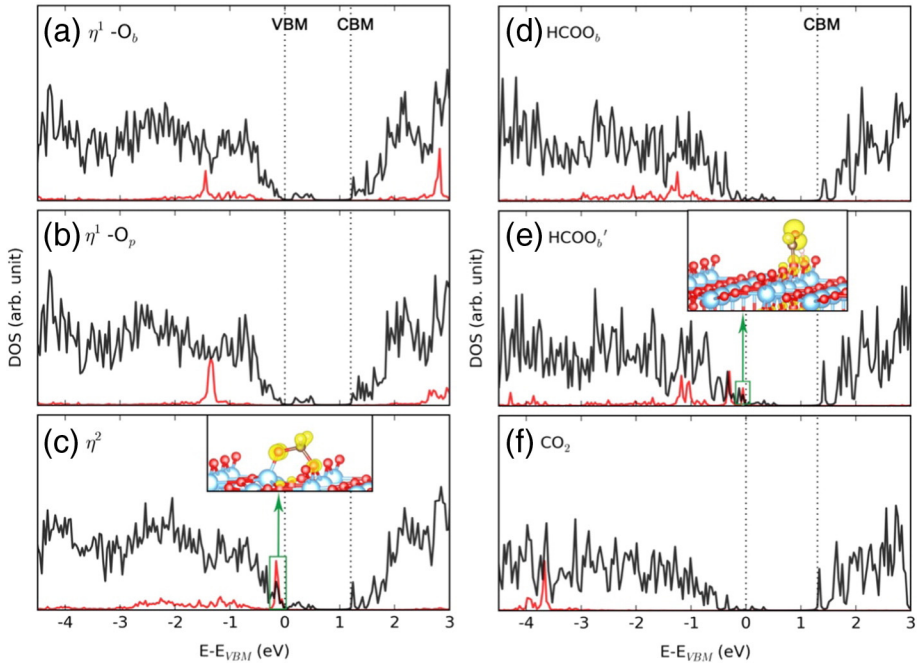

Fig. 5. Total (black) and partial (red) DOS of the reactants (HCHO), intermediates ($HCOO_b$ and $HCOO_b'$) and product (CO_2) on rutile TiO_2(110) surface. For those systems which have high photocatalytic reactivity (c and e), the orbital spatial distribution of adsorbate HOMO is presented in the inset.

Please cite this article as: L. Liu, J. Zhao, Formaldehyde adsorption and decomposition on rutile (110): A first-principles study, Surf. Sci. (2016), http://dx.doi.org/10.1016/j.susc.2015.12.036

3.3. Photocatalytic reactivity

Since TiO_2 is a widely used photocatalytic material, it is also very important to understand its photocatalytic reactivity. The thermal catalytic reactions and photocatalytic reactions are often combined together in the experimental measurements and practical applications [23–25].

Photocatalytic activity depends on the optimal alignment of electronic levels at the molecule–semiconductor interface [40–43]. When an adsorbed molecule has the highest occupied molecular orbital (HOMO) or lowest unoccupied molecular orbital (LUMO) in the band gap or at least close to valance band maximum (VBM) or conduction band minimum (CBM) of TiO_2, it has high photocatalytic reactivity. Therefore, we investigate the energy level alignment based on the calculations of total and partial density of states (DOS) for the stable reactant (HCHO), intermediates ($HCOO_b$ and $HCOO_b'$) and product (CO_2) in the decomposition of HCHO on rutile TiO_2(110) surface. The bottom Ti-O-Ti tri-layer contains unsaturated two-coordinated O (O_{2C}) and Ti_{5C} with bulk-like structure which contributes artificial DOS [44]. Therefore, in the calculations of total DOS, we subtract the contribution of the bottom Ti-O-Ti tri-layer. In this report, the electronic structure is calculated at the DFT level using PBE functional. It is well-known that DFT underestimates the band gap due to the lack of self-interaction correction. However, based on our previous energy level alignment investigations of H_2O and CH_3OH on TiO_2, we found that although DFT-PBE does not give the correct band gap, it provides the energy level alignment agrees qualitatively with many-body quasiparticle GW results [40–43]. Therefore, in this report, we use DFT with PBE functional to investigate the energy level alignment.

The total and partial DOS is shown in Fig. 5. To make the partial DOS contributed by the adsorbate more visible, it is expanded by 5 times. The VBM and CBM is marked using dotted lines. First, as shown in Fig. 5, the LUMOs of the adsorbates all have energies more than 1.5 eV higher than CBM, meaning that the photo-reduction induced by excited electrons is difficult. In contrast, two of the adsorbed structures have HOMOs very close to VBM, suggesting a good reactivity for photo-oxidation. Fig. 5(a–c) give the total and partial DOS of HCHO on rutile TiO_2(110) surface with monodentate and bidentate configurations. One can see that the HOMO of monodentate η^1-O_b and η^1-O_p is at around −1.5 eV below VBM. In contrast, bidentate η^2 has its HOMO only 0.1 eV below VBM. This suggests that bidentate η^2 configuration is a possible hole trapping site. Compared with CH_3OH, HCHO with η^2 structure has better hole scavenger properties [40]. In the inset of Fig. 5(c), we plot out the orbital distribution of the HOMO of HCHO as the hole acceptor level. We found that it is the π* orbital hybridized by the *2p* orbitals from C_m, O_m and O_b. The *Ti_3d* orbital also has a small contribution. Trapping an excited hole may lower the breaking-bond energy barriers of C_m-O_m C_m-O_b or Ti_{5c}-O_m bonds. We propose that by breaking the C_m-O_m and C_m-O_b bonds simultaneously, an intermediate CH_2 can be generated from the surface. If there are two neighboring HCHO, C_2H_4 could be produced. This qualitatively explains the observation of C_2H_4 in the XPS and TPD experiments [23,24]. The hole trapping may also help the transition from the bidentate η^2 configuration to monodentate η^1 configuration by breaking the C_m-O_b bond. Because of the contribution of *Ti_3d* orbital, for η^2 configuration, Ti-O_m bond break, e.g., the transition from HCHO to $HCOO_b$ could also be easier.

Fig. 5(d–f) show the total and partial DOS of adsorbed $HCOO_b$, $HCOO_b'$ and CO_2. One can see that HOMO of CO_2 is as low as −3.7 eV below VBM, suggesting a very low photocatalytic reactivity. The HOMO of $HCOO_b$ is also at −1.2 eV below VBM. In contrast, the $HCOO_b'$ intermediate has its HOMO just at VBM, implying it to be a hole scavenger. In the inset of Fig. 5(e), we plot the orbital distribution of $HCOO_b'$ HOMO. It is also mainly the π* orbital hybridized by the *2p* orbitals of C_m and O_m. The H and O_b atoms also have small contribution. Trapping an excited hole may help to break the C_m-O_m, C_m-O_b or C_m-H bonds. It could induce the desorption of $HCOO_b'$ from the surface and help the second deprotonation to generate CO_2.

4. Conclusions

Trying to understand the thermal catalytic and photocatalytic properties of HCHO on TiO_2, we performed a systematic study based on first-principles calculations. First, we investigated the adsorption structures of HCHO on stoichiometric rutile TiO_2(110) surface. We confirmed three different adsorption structures containing one bidentate and two monodentate configurations. The two monodentate configurations are almost degenerate in energy. The bidentate configuration is the most stable one because of one additional C_m-O_b bond formation and the orbital hybridization changing from sp^2 to sp^3. The energy difference and conversion energy barrier between the bidentate and monodentate configurations depend on the adsorption coverage. Second, we studied the thermal decomposition of HCHO to CO_2 from different adsorption structures on stoichiometric rutile TiO_2(110) surface. The decomposition includes two deprotonation processes. The energy barrier of the first deprotonation is 1.3 eV and 1.1 eV for bidentate and monodentate configurations. After the first deprotonation, an adsorbed formate $HCOO_b$ specie is formed. The second deprotonation needs 1.74 eV and 1.64 eV for bidentate and monodentate configurations. An intermediate $HCOO_b'$ can be generated from bidentate configuration. After that, an adsorbed CO_2 is formed. It can desorb from the surface after overcoming a small barrier of 0.12 eV. In principle, it is also possible to obtain a CO molecule from the surface. Yet a large energy barrier around 1.8 eV needs to be overcome. Third, by analyzing the energy alignment of molecular orbitals with TiO_2 energy band edges, we discussed the photocatalytic activity of the reactants and intermediates during the decomposition process. We found that the adsorbed HCHO with bidentate configuration and the intermediate $HCOO_b'$ have high photocatalytic reactivity. Trapping the excited holes may help the conversion between the bidentate and monodentate configurations and the generation of C_2H_4. Our results apply a clear description to the adsorption structure and thermal decomposition process of HCHO on rutile TiO_2(110) surface. The band alignment discussion provides valuable insights to understand the combined photocatalytic and thermally catalytic reactions of HCHO on rutile TiO_2(110) surface.

Acknowledgements

This work is supported by NSFC (21373190, 11322434, 21421063), by National Key Basic Research Program (2011CB921404) and USTC funding WK2030020027. Calculations were performed at the Shanghai Supercomputer Center and Environmental Molecular Sciences Laboratory at the PNNL, a user facility sponsored by the DOE Office of Biological and Environmental Research.

References

[1] A. Fujishima, K. Honda, Nature 238 (1972) 37.
[2] B. Oregan, M. Gratzel, Nature 353 (1991) 737.
[3] M. Valden, S. Pak, X. Lai, D.W. Goodman, Catal. Lett. 56 (1998) 7.
[4] M. Valden, X. Lai, D.W. Goodman, Science 281 (1998) 1647.
[5] M.S. Chen, D.W. Goodman, The structure of catalytically active gold on titania, Science 306 (2004) 252.
[6] M.S. Chen, D.W. Goodman, Acc. Chem. Res. 39 (2006) 739.
[7] U. Diebold, Surf. Sci. Rep. 48 (2003) 53.
[8] M.A. Henderson, I. Lyubinetsky, Chem. Rev. 113 (2013) 4428.
[9] U. Diebold, Appl. Phys. A Mater. Sci. Process. 76 (2003) 681.
[10] M. Ni, M.K.H. Leung, D.Y.C. Leung, K. Sumathy, Renew. Sust. Energ. Rev. 11 (2007) 401.
[11] A. Fujishima, X. Zhang, D. Tryk, Surf. Sci. Rep. 63 (2008) 515.
[12] C.H. Sun, L.M. Liu, A. Selloni, G.Q. Lu, S.C. Smith, J. Mater. Chem. 20 (2010) 10319.
[13] L.M. Liu, P. Crawford, P. Hu, Prog. Surf. Sci. 84 (2009) 155.
[14] A.L. Linsebigler, G.Q. Lu, J.T. Yates, Mech. Sel. Results Chem. Rev. 95 (1995) 735.
[15] T.L. Thompson, J.T. Yates, Chem. Rev. 106 (2006) 4428.
[16] I.X. Green, W.J. Tang, M. Neurock, J.T. Yates, Science 333 (2011) 736.
[17] Z. Zhang, J.T. Yates, Chem. Rev. 112 (2012) 5520.
[18] J.T. Yates, Surf. Sci. 603 (2009) 1605.
[19] M. Pelaez, N.T. Nolan, S.C. Pillai, M.K. Seery, P. Falaras, A.G. Kontos, P.S.M. Dunlop, J.W.J. Hamilton, J.A. Byrne, K. O'Shea, M.H. Entezari, D.D. Dionysiou, Appl. Catal. B Environ. 125 (2012) 331.

Please cite this article as: L. Liu, J. Zhao, Formaldehyde adsorption and decomposition on rutile (110): A first-principles study, Surf. Sci. (2016), http://dx.doi.org/10.1016/j.susc.2015.12.036

[20] J.L. Bronkema, D.C. Leo, A.T. Bell, J. Phys. Chem. C 111 (2007) 14530.
[21] Q. Guo, C.B. Xu, W.S. Yang, Z.F. Ren, Z.B. Ma, D.X. Dai, T.K. Minton, X.M. Yang, J. Phys. Chem. C 117 (2013) 5293.
[22] Q. Yuan, Z. Wu, Y. Jin, L. Xu, F. Xiong, Y. Ma, W. Huang, J. Am. Chem. Soc. 135 (2013) 5212.
[23] Q. Yuan, Z. Wu, Y. Jin, F. Xiong, W. Huang, J. Phys. Chem. C 118 (2014) 20420.
[24] C. Xu, W. Yang, Q. Guo, D. Dai, T.K. Minton, X. Yang, J. Phys. Chem. Lett. 4 (2013) 2668.
[25] K.R. Phillips, S.C. Jensen, M. Baron, S.C. Li, C.M. Friend, J. Am. Chem. Soc. 135 (2013) 574.
[26] Z. Zhang, M. Tang, Z.-T. Wang, Z. Ke, Y. Xia, K.T. Park, I. Lyubinetsky, Z. Dohnálek, Q. Ge, Top. Catal. (2014).
[27] K. Zhu, Y. Xia, M. Tang, Z.-T. Wang, B. Jan, I. Lyubinetsky, Q. Ge, Z. Dohnálek, K.T. Park, Z. Zhang, J. Phys. Chem. C 150610131754005 (2015).
[28] K. Zhu, Y. Xia, M. Tang, Z.-T. Wang, I. Lyubinetsky, Q. Ge, Z. Dohnálek, K.T. Park, Z. Zhang, J. Phys. Chem. C 119 (2015) 18452.
[29] L. Kieu, P. Boyd, H. Idriss, J. Mol. Catal. A Chem. 176 (2001) 117.
[30] J. Haubrich, E. Kaxiras, C.M. Friend, Chemistry 17 (2011) 4496.
[31] H. Liu, X. Wang, C. Pan, K.M. Liew, J. Phys. Chem. C 116 (2012) 8044.
[32] Z.R. Zhang, M.R. Tang, Z.T. Wang, Z. Ke, Y.B. Xia, K.T. Park, I. Lyubinetsky, Z. Dohnalek, Q.F. Ge, Top. Catal. 58 (2015) 103.
[33] G. Kresse, J. Furthmuller, Phys. Rev. B 54 (1996) 11169.
[34] G. Kresse, J. Hafner, Phys. Rev. B 48 (1993) 13115.
[35] J.P. Perdew, M. Emzerhof, K. Burke, J. Chem. Phys. 105 (1996) 9982.
[36] J.P. Perdew, K. Burke, M. Ernzerhof, Phys. Rev. Lett. 77 (1996) 3865.
[37] P.E. Blochl, Phys. Rev. B 50 (1994) 17953.
[38] G. Kresse, D. Joubert, Phys. Rev. B 59 (1999) 1758.
[39] G. Henkelman, B.P. Uberuaga, H. Jonsson, J. Chem. Phys. 113 (2000) 9901.
[40] A. Migani, D.J. Mowbray, A. Iacomino, J. Zhao, H. Petek, A. Rubio, J. Am. Chem. Soc. 135 (2013) 11429.
[41] A. Migani, D.J. Mowbray, J. Zhao, H. Petek, A. Rubio, J. Chem. Theory Comput. 10 (2014) 2103.
[42] A. Migani, D.J. Mowbray, J. Zhao, H. Petek, J. Chem. Theory Comput. 11 (2015) 239.
[43] H. Sun, D.J. Mowbray, A. Migani, J. Zhao, H. Petek, A. Rubio, ACS Catal. 5 (2015) 4242.
[44] P.M. Kowalski, B. Meyer, D. Marx, Phys. Rev. B 79 (2009).

Please cite this article as: L. Liu, J. Zhao, Formaldehyde adsorption and decomposition on rutile (110): A first-principles study, Surf. Sci. (2016), http://dx.doi.org/10.1016/j.susc.2015.12.036